

Giant spin-dependent photo-conductivity in GaAsN dilute nitride semiconductor

A. Kunold¹, A. Balocchi², F. Zhao², T. Amand², N. Ben Abdallah³, J. C. Harmand⁴, X. Marie²

¹*Departamento de Ciencias Básicas, Universidad Autónoma Metropolitana-Azcapotzalco, Av. San Pablo 180, Col. Reynosa Tamaulipas, México D.F., México*

²*Université de Toulouse; INSA-CNRS-UPS, LPCNO, 135, Av. de Rangueil, 31077 Toulouse, France*

³*Université de Toulouse; UPS-CNRS-INSa, IMT, 118, route de Narbonne, 31062 Toulouse cedex 04, France*

⁴*CNRS-LPN, Route de Nozay, 91460 Marcoussis, France*

A theoretical and experimental study of the spin-dependent photoconductivity in dilute Nitride GaAsN is presented. The non linear transport model we develop here is based on the rate equations for electrons, holes, deep paramagnetic and non paramagnetic centers both under CW and pulsed optical excitation. Emphasis is given to the effect of the competition between paramagnetic centers and non paramagnetic centers which allows us to reproduce the measured characteristics of the spin-dependent recombination power dependence. Particular attention is paid to the role of an external magnetic field in Voigt geometry. The photoconductivity exhibits a Hanle-type curve whereas the spin polarization of electrons shows two superimposed Lorentzian curves with different widths, respectively related to the recombination of free and trapped electrons. The model is capable of reproducing qualitatively and quantitatively the most important features of photoluminescence and photocurrent experiments and is helpful in providing insight on the various mechanisms involved in the electron spin polarization and filtering in GaAsN semiconductors.

I. INTRODUCTION

The dependence of the recombination time on the relative spin orientation of photogenerated carriers on paramagnetic centers, namely the spin dependent recombination (SDR) has been known for over 50 years since the first optically detected magnetic resonance (ODMR) experiments carried out by Geschwind *et al.*¹ in Al₂O₃. It has been observed in surface centers on crystalline silicon^{2,3} and on several systems including dislocated silicon⁴, amorphous silicon⁵ and later on in (Al)GaAs⁶⁻⁸. In dilute nitride GaAsN samples SDR has been evidenced with record high values at room temperature in photoluminescence (PL) experiments⁹⁻¹³ and recently in photoconductivity (PC) measurements¹⁴, stimulating new applications of the SDR as a light- or electron spin-polarization detector. Furthermore it has been shown by ODMR that it is in fact Nitrogen-induced Gallium self interstitial deep paramagnetic centers, and not Nitrogen itself, which harness the SDR in GaAsN alloys¹⁵.

The key point in the SDR effect is the existence of deep centers inside the gap possessing an unpaired electron at equilibrium (paramagnetic centers). As a consequence, if a photogenerated electron in the conduction band and the resident electron on the deep center have the same spin, the photogenerated electron cannot be captured by the center (it is generally assumed that the triplet levels are not bound). On the contrary, when the photogenerated electrons and the the deep center resident electron have antiparallel spins, the capture is efficient. Therefore the recombination time of photocreated electrons depends on the relative orientation of the free electron and of the unpaired electron resident on the center. After the capture the centers annihilate one of the two electrons through a spin-independent recombination with an unpolarized hole. Under the influence of linearly polarized light an equal number of spin up and spin down

conduction band electrons are created which are likewise captured by the paramagnetic centers. However, under circularly polarized light one given conduction band electron spin orientation is preferred over the other. This not only creates spin polarized conduction band electrons through the usual selection rules but also dynamically polarizes centers. By both removing conduction band electrons with opposite spin orientation and by blocking the equally polarized ones, this mechanism gives rise to very high and very long living conduction band electron spin polarization and to larger PL intensities under circularly polarized light compared to those under linearly polarized excitation^{6,7,10,11}.

The theoretical work on SDR can be divided into two groups: stochastic Liouville equation^{16,17}, mostly devoted to silicon, and rate equations^{6,7,10,15,18,19} which have been used to study SDR in silicon as well as in GaAs(N). The former focuses mainly in the process of formation and dissociation of electron pairs in centers while the latter studies the conduction band carrier recombination into centers and valence band states. Haberkorn *et al.*¹⁷ studied the process of formation and dissociation of paired spin-up and spin-down electrons via the solution of the stochastic Liouville equation including the Zeeman part of the Hamiltonian and a stochastic linear term. Similar models also include interaction terms between the electron spins. These models are suitable to the understanding of ODMR and similar experiments. Weisbuch *et al.*⁶ and Kalevich *et al.*^{10,12,13} studied the recombination dynamics of carriers through a rate equations model that considers spin up and spin down electrons coupled to a distribution of paramagnetic centers constituting the SDR channel. In later approaches an equivalent set of rate differential equations for the spin variables of electrons and centers as well as the populations of free and trapped carriers was proposed^{12,13}, lacking however the recombination through non param-

agnetic centers which is important to interpret the power dependence of SDR phenomena.

In this paper we present a comprehensive theoretical and experimental work on SDR related phenomena in GaAsN, mainly focusing on photocurrent experiments. We have developed a new non-linear transport model based on rate equations for electrons, holes and deep paramagnetic centers in GaAsN based on the initial model proposed to explain the strong SDR effects measured in photoluminescence experiments^{12,13,15,18,20}. We show that the electron recombination to non-paramagnetic centers, which was neglected in the first models, is essential to understand the SDR dependence as a function of the excitation power. The proposed theoretical model is able to reproduce accurately the most important features of both PC and PL experiments. Finally we have measured and modeled the variation of the spin-dependent photoconductivity and photoluminescence signals as a function of an external magnetic field in Voigt configuration. As expected, the SDR effect decreases when the amplitude of the external field increases. The spin-dependent photoconductivity signal exhibits clearly a Hanle like curve, well described by the theoretical model.

The paper is organized as follows. The next section presents the samples' characteristics and the experimental setup. We begin by discussing a previously formulated rate equations model^{12,13} in Sec. III which is suitable to understand PL experiments. Starting from this system of differential equations we develop the model to include non SDR channels in the form of non paramagnetic centers in Sec. III A and a uniform external magnetic field in Sec. III B. These preliminary parts put the fundamentals for the interpretation and modelization of the SDR mediated transport phenomena developed in Sec. III C. Here we put forward a nonlinear system of partial differential equations by introducing drift terms for the conduction band electrons and valence band holes. Sec. IV begins with a brief description of the numerical methods used to solve the system of partial differential equations obtained in the previous section. We discuss here two main results on transport experiments and calculations: the SDR as a function of the incident laser power and applied magnetic field. Our main results are summarized in Sec. V.

II. SAMPLES AND EXPERIMENTAL SET-UP

The samples under study were grown under the same conditions by molecular beam epitaxy at $T = 410^\circ\text{C}$ on (001) semi-insulating GaAs substrates, after a 400nm GaAs buffer layer. They consist of GaAsN semiconductor epilayers of different Nitrogen content and thickness. Sample A has a nominally undoped 50nm thick $\text{GaAs}_{0.981}\text{N}_{0.019}$ epilayer, sample B has a nominally undoped 100nm thick $\text{GaAs}_{0.9924}\text{N}_{0.0076}$ epilayer and sample C a 50nm thick Si modulation doped (doping density 10^{18} cm^{-3}) $\text{GaAs}_{0.979}\text{N}_{0.021}$ epilayer. The growth

was terminated with a 10nm GaAs cap layer and no post growth rapid thermal annealing was performed. We have observed similar effects in other doped or undoped samples with N composition varying in the range 0.7% to 2.6%.

The excitation light was provided by a Ti:Sa laser, propagating along the direction normal to the sample surface, either in mode-locked regime, yielding the generation of 1.5ps pulses at a repetition frequency of 80MHz, or in continuous wave operation, at a wavelength $\lambda_{exc} = 840\text{nm}$. The laser was focused to a $\sim 150\mu\text{m}$ or $\sim 40\mu\text{m}$ diameter spots respectively in between two Ag electrodes deposited onto the sample surface $\sim 0.8\text{mm}$ apart or between two ohmic contacts of variable shape and dimension defined by lithographic techniques and contacted by ultrasonic wire bonding. The laser light used for the photo excitation is either circularly polarized (right σ^+ or left σ^-) or linearly (σ^X or σ^Y) polarized along a direction perpendicular to the surface of the sample (\mathbf{k}) and modulated by a mechanical chopper. The sample conductivity was then measured using a synchronous lock-in amplifier from the voltage drop at the terminals of a $10\text{k}\Omega$ load resistor placed in series with the sample. A constant voltage in the range $0 < V < 12$ volts was applied between the sample electrodes. The PL intensity was simultaneously measured with the same lock-in technique by recording its total intensity filtered of the laser scattered light, and integrated by a silicon p-i-n photodiode. All the experiments have been performed at room temperature.

III. MODEL

In GaAsN samples illuminated by linearly polarized light, identical populations of spin-up and spin-down electrons are photogenerated in the conduction band and are subsequently captured by paramagnetic centers containing an electron with opposite spin. The newly formed pairs dissociate at the centers leaving the same population of spin up and spin down paramagnetic centers as well. On the contrary, under circularly polarized excitation σ^- (σ^+) approximately 75% of the photogenerated electrons are spin-up (spin-down) polarized and 25 % are spin-down (spin-up) polarized given the optical selection rules in GaAs²¹. Thus, most of the processes occurring in the SDR channel will correspond, under σ^+ excitation, to spin down conduction electrons rapidly recombining in spin up paramagnetic traps leaving most of the spin-down centers unpaired. After a few cycles the population of spin-up traps will be considerably depleted. This has the effect of a double spin filter: first, photogenerated spin-down electrons are prevented from recombining and second, electrons which undergo spin flipping mechanism are rapidly removed from the conduction band by the traps owing to the high availability of matching centers. Moreover, the minority spin-up centers can efficiently trap a spin-down electron increasing the centers' spin polariza-

tion, so that the whole spin system is self-containing. At this stage the SDR channel is almost closed and the electrons-hole recombination through band to band optical transitions becomes more probable, increasing the photoluminescence yield. Moreover, as a result of the highly populated conduction band, a higher photoconductivity is expected under circular polarization compared to linear excitation.

We start with the rate equations model originally proposed by Kalevich *et al.*^{12,13,18} which grasps the essential features of the SDR effect:

$$\frac{\partial n_{\pm}}{\partial t} = \frac{n_{\mp} - n_{\pm}}{2\tau_s} - \gamma_e n_{\pm} N_{\mp} + G_{\pm}, \quad (1)$$

$$\frac{\partial p}{\partial t} = -\gamma_h p N_2 + G, \quad (2)$$

$$\frac{\partial N_{\pm}}{\partial t} = \frac{N_{\mp} - N_{\pm}}{2\tau_{sc}} - \gamma_e n_{\mp} N_{\pm} + \frac{\gamma_h p N_2}{2}, \quad (3)$$

$$\frac{\partial N_2}{\partial t} = \gamma_e (n_+ N_- + n_- N_+) - \gamma_h p N_2. \quad (4)$$

Here the subindices + and - stand for spin polarized electrons with spin projection $+\hbar/2$ and $-\hbar/2$ respectively along the incident light axis, thus n_+ and n_- are the number of spin-up and spin-down conduction band electrons of total number $n = n_+ + n_-$. Similarly N_+ and N_- are the the spin-up and spin-down paramagnetic traps. The total number of unpaired paramagnetic traps is given by $N_1 = N_+ + N_-$ and N_2 is the total number of electrons singlets hosted by the paramagnetic traps. Holes (p) are considered unpolarized as their spin relaxation time is shorter than 1ps at room temperature²² due to the fourfold degeneracy of the valence band at $k = 0$ and the large spin-orbit coupling in III-V semiconductors. Eqs. (1)-(4) ensure conservation of charge neutrality and number of centers:

$$n - p + N_2 = 0, \quad (5)$$

$$N_1 + N_2 = N. \quad (6)$$

The terms of the form $-\gamma_e n_{\pm} N_{\mp}$ are responsible for the spin dependent free electron capture in paramagnetic centers with recombination rate γ_e while the terms $-\gamma_h p N_2$ model the spin independent recombination of one electron of the paramagnetic center singlet with a hole. The structure of these terms guarantees that spin-up conduction band electrons will only be trapped by spin-down centers and viceversa in order to comply with the Pauli exclusion principle. This recombination is at the heart of SDR mechanism: under σ^+ polarized excitation, for instance, the N_- population builds up and the N_+ population is symmetrically quenched due to the spin dependent electron recombination on paramagnetic centers. Values of the spin relaxation time of free and unpaired electrons on the centers $\tau_s = 130ps$ and $\tau_{sc} = 2000ps$ respectively and the effective hole life time $\tau_h = 35ps$ as well as the typical ratio of the electron to the hole recombination coefficients $\gamma_e/\gamma_h = 10$ (where $\gamma_h = 1/\tau_h N$) are estimated from previous time resolved PL experiments^{10,18}.

The photo generation of electrons is accounted for by the terms G_+ and G_- and of holes by $G = G_+ + G_-$. Under CW excitation the generation term per unit surface is taken as

$$G_{\pm}(t) = \frac{\alpha LP}{2\hbar\omega_{\nu}} \left\{ 1 \pm S_0 \left[1 + \tanh\left(\frac{t-t_0}{s_t}\right) \right] \right\} \quad (7)$$

where P is the laser irradiance, $h\nu$ is the photon's energy, $2S_0$ is the maximum polarization degree of the generated electrons, α is the absorption coefficient of GaAs and L is the width of the GaAsN layer. The excitation light polarization is gradually switched from linear ($S_0 = 0$) to circular ($S_0 = 1/2$) by the tanh function; the s_t parameter specifies the switching time between the the linearly ($S_z=0$) and circularly polarized excitation ($S_z = S_0$). given the optical selection rules for GaAs under a non resonant excitation involving only the valence band $s = 3/2$ levels, the polarization of the generation term is set to $S_0 = 1/4$ when the polarization of light is 100% circular. Under pulsed excitation the generation terms are given by

$$G_{\pm}(t) = \frac{\alpha LP t_{pp}}{\sqrt{2\pi\hbar\omega_{\nu} s_t}} (1 \pm 2S_0) e^{-\frac{(t-t_0)^2}{2s_t^2}}, \quad (8)$$

where P is the laser's time average irradiance for pulses of period t_{pp} and width s_t . In our experiments $t_{pp} = 12ns$ and $s_t = 1.5ps$.

In CW conditions the total photoluminescence intensity under linear (X) or circular (+) excitation is calculated as $I_{X,+} = \gamma_r n(t) p(t)$ where γ_r is the optical recombination rate and t is a sufficiently long time to insure that the steady state has been reached. Under pulsed excitation the photoluminescence intensity is calculated as the time average $I_{X,+} = \gamma_r \int_0^{t_{pp}} n(t) p(t) dt / t_{pp}$. The total PL acts only as a probe of SDR effect here, since it weakly modifies the n and p densities²³.

A convenient pointer of SDR related phenomena is the SDR ratio (SDR_r) which is given by the quotient of the total photoluminescence intensity under circularly polarized excitation to the total photoluminescence intensity under linearly polarized excitation. The photoluminescence SDR ratio is thus defined as

$$SDR_r = \frac{I_+}{I_X}. \quad (9)$$

In the absence of the SDR mechanism, $SDR_r = 1$ whereas in its presence $SDR_r > 1$. In photocurrent experiments we replace the photoluminescence intensity by the photocurrent in the definition of SDR_r given that larger photocurrents are expected in the presence of circularly polarized light.

A. Non-SDR channels: Non paramagnetic centers

Although the main features of the SDR effect in dilute Nitrides such as the very long conduction electrons

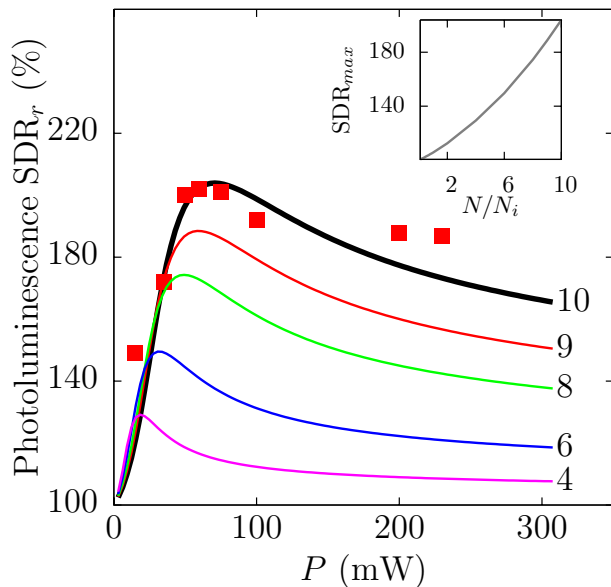


FIG. 1. (color on line) Photoluminescence SDR ratio vs laser power P for various ratios of the paramagnetic to non paramagnetic center of $N/N_i = 4$ (purple), 6 (blue), 8 (green), 9 (red) and 10 (black). The (red) squares indicate the experimental results. The dependence of the SDR maximum SDR_{max} as a function of N/N_i is shown in the inset.

effective spin life time (in time resolved photoluminescence experiments)^{15,18} are well described by the model above, it fails to reproduce the power dependence of the SDR ratio²⁰. Fig. 1 shows the photoluminescence measurement [(red) squares] for sample A in the pulsed excitation regime and theoretical calculations [(black) solid line] of the SDR_r as a function of the laser power. The data shows a steep increase of the SDR_r as a function of the incident power, up to an optimum value. Above this power, the SDR_r smoothly but monotonously decreases. This is clearly due to the competition between SDR and non-SDR channels. In the low power regime ($P < 50\text{mW}$) the SDR mechanism dynamically polarizes the spin of paramagnetic centers thus blocking the recombination of spin polarized conduction band electrons with the same spin orientation and filtering out oppositely spin polarized ones. Once the optimum power is reached ($P \approx 75\text{mW}$ in Fig. 1) most of the paramagnetic centers are spin polarized. For higher laser powers the SDR mechanism is overwhelmed by the larger number of generated conduction band electrons and the recombination through non paramagnetic centers dominates.

This competition mechanism is a non linear contribution that has an important role at high excitation power and was not considered in the first models developed to interpret the remarkable spin properties of GaAsN^{12,13,18}. The presence of such centers is attested by the observation of numerous peaks in infrared spectroscopy²⁴. Introducing this mechanism into the pre-

vious set of rate equations we obtain

$$\frac{\partial n_{\pm}}{\partial t} = \frac{n_{\mp} - n_{\pm}}{2\tau_s} - \gamma_e n_{\pm} N_{\mp} - \gamma_a n_{\pm} (N_i - N_3) + G_{\pm}, \quad (10)$$

$$\frac{\partial p}{\partial t} = -\gamma_h p N_2 - \gamma_b p N_3 + G, \quad (11)$$

$$\frac{\partial N_{\pm}}{\partial t} = \frac{N_{\mp} - N_{\pm}}{2\tau_{sc}} - \gamma_e n_{\mp} N_{\pm} + \frac{\gamma_h p N_2}{2}, \quad (12)$$

$$\frac{\partial N_2}{\partial t} = \gamma_e (n_+ N_- + n_- N_+) - \gamma_h p N_2, \quad (13)$$

$$\frac{\partial N_3}{\partial t} = \gamma_a (N_i - N_3) n - \gamma_b p N_3. \quad (14)$$

Here N_i and N_3 are the number of total and occupied non-paramagnetic centers respectively; γ_a is the recombination rate of conduction band electrons to non paramagnetic centers and γ_b is the recombination rate of non-paramagnetic centers to valence band.

Assuming that the non paramagnetic centers have the same recombination rates as paramagnetic centers (i.e. $\gamma_a/\gamma_e \approx 1$ and $\gamma_b/\gamma_h \approx 1$), the main adjustable parameter of our model is the total number of non paramagnetic centers. Their role is clearly evidenced in Fig. 1. In this graph we present a series of SDR_r vs power curves for various rates of paramagnetic centers to non paramagnetic centers N/N_i keeping N constant. As N/N_i increases, the SDR_r maximum increases and moves to higher irradiance values. As the number of non paramagnetic centers is increased, the effective conduction electron recombination time $1/\gamma_a N_i$ [see Eq. (10)] is shortened making this mechanism more likely at lower laser irradiance. At the same time the SDR maximum ratio is reduced as a consequence of the increasing transit of non polarized electrons through the non paramagnetic centers¹⁵. The best agreement with the experimental results for sample A (Fig. 1) is achieved with $N_i = N/10$ where the total paramagnetic center density $N = N_+ + N_- + N_2$ is kept constant. The fitting of the PL SDR_r power dependence allows us to fix the ratio N/N_i to be used in the following photoconductivity model.

B. Effect of a magnetic field

In order to include magnetic field effects into the model, we first recall the simple case of a spin 1/2 particle coupled to the magnetic field via the Zeeman Hamiltonian

$$H = \hbar\omega \cdot \mathbf{s} \quad (15)$$

where $\omega = g\mu_B\hbar\mathbf{B}$, g is the gyromagnetic factor of free electrons, μ_B is the Bohr magneton and \mathbf{s} is the dimensionless vector spin operator for the particle. By solving the von Neumann equation for the density matrix and averaging the spin vector one finds that the Hamiltonian (15) yields the well known coherent term contribution for

the total spin evolution

$$\frac{d\mathbf{S}}{dt} = \boldsymbol{\omega} \times \mathbf{S}. \quad (16)$$

The spin component along the propagation of light direction is related to the number of spin-up and spin-down electrons in \hbar units through $S_z = (n_+ - n_-)/2$ ^{12,13}.

For the trapped electrons we can work out a similar dynamical equation given by

$$\frac{d\mathbf{S}_c}{dt} = \boldsymbol{\Omega} \times \mathbf{S}_c. \quad (17)$$

where $\boldsymbol{\Omega} = g_c \mu_B \hbar \mathbf{B}$ with g_c the gyromagnetic factor for trapped electrons and the spin component along the z axis is $S_{zc} = (N_+ - N_-)/2$. The gyromagnetic factors for free electrons and trapped electrons were set to $g = 0.5$ and $g_c = 2$ respectively^{12,13,25,26}.

Subtracting Eq. (10) for spin-down to spin-up electrons and adding the term (16) for spin precession we obtain

$$\begin{aligned} \frac{dS_z}{dt} + \frac{\gamma_e}{2} (nN_1 - 4S_z S_{zc}) + \frac{1}{\tau_s} S_z \\ + (\mathbf{S} \times \boldsymbol{\omega})_z = \frac{G_+ - G_-}{2}. \end{aligned} \quad (18)$$

where we have used the identity

$$n_+ N_- + n_- N_+ = \frac{1}{2} (nN_1 - 4S_z S_{zc}). \quad (19)$$

Adding Eq. (10) for spin-up and spin-down electrons considering isotropic spin relaxation time τ_s we obtain the rate equation for the total number of conduction band electrons. An analogous procedure is followed for the paramagnetic center variables.

Finally the whole set of rate equations for the spin variables, total conduction band and trapped electrons is given by

$$\begin{aligned} \dot{\mathbf{S}} + \frac{\gamma_e}{2} (\mathbf{S} N_1 - \mathbf{S}_c n) + \frac{\gamma_a}{2} \mathbf{S} (N_i - N_3) \\ + \frac{1}{\tau_s} \mathbf{S} + \mathbf{S} \times \boldsymbol{\omega} = \boldsymbol{\Delta G}, \end{aligned} \quad (20)$$

$$\dot{\mathbf{S}}_c + \frac{\gamma_e}{2} (\mathbf{S}_c n - \mathbf{S} N_1) + \frac{1}{\tau_{sc}} \mathbf{S}_c + \mathbf{S} \times \boldsymbol{\Omega} = \mathbf{0}, \quad (21)$$

$$\begin{aligned} \dot{n} + \frac{\gamma_e}{2} (nN_1 - 4\mathbf{S} \cdot \mathbf{S}_c) \\ + \gamma_a n (N_i - N_3) = G, \end{aligned} \quad (22)$$

$$\dot{p} + \gamma_h N_2 p - \gamma_b p N_3 = G, \quad (23)$$

$$\dot{N}_1 + \frac{\gamma_e}{2} (nN_1 - 4\mathbf{S} \cdot \mathbf{S}_c) - \gamma_h N_2 p = 0, \quad (24)$$

$$\dot{N}_2 - \frac{\gamma_e}{2} (nN_1 - 4\mathbf{S} \cdot \mathbf{S}_c) + \gamma_h N_2 p = 0, \quad (25)$$

$$\dot{N}_3 = \gamma_a (N_i - N_3) n - \gamma_b p N_3 \quad (26)$$

where $\boldsymbol{\Delta G} = (G_+ - G_-)\mathbf{k}/2$. In an isotropic media the dynamical equations for the three spin components

should be invariant under rotations, hence we have replaced $nN_1 - 4S_z S_{zc}$ by $nN_1 - 4\mathbf{S} \cdot \mathbf{S}_c$. By doing this the recombination rate of conduction electrons to paramagnetic centers is increased when \mathbf{S} and \mathbf{S}_c are antiparallel whereas it vanishes when they are parallel as expected from the Pauli exclusion principle needed to form a singlet state.

C. Photoconductivity

Having defined the most important generation terms we turn to the central problem of this work: electron transport combined with SDR effects.

Modulation of the photoconductivity with the polarization of the excitation light up to 40% has been indeed measured very recently at $T = 300$ K¹⁴.

Several theoretical contributions have been presented to study the transport of electrons in doped GaAsN²⁷. Fahy *et al.* used a tight binding model and the Boltzmann equation in the relaxation-time approximation to obtain the mobility of conduction band electrons in GaAsN²⁷. Nevertheless the spin degree of freedom was not considered in this work.

In order to focus on SDR associated phenomena we present a simpler approach in which the electron and hole density currents are introduced through drift terms for the current neglecting other transport phenomena as diffusion. The Einstein-Smoluchowski relation for the diffusion coefficient yields a diffusion length of a few hundred nanometers compared to the laser spot size in the order of the $100\mu m$ due to the low mobility ($\mu \approx 100$ cm²/Vs²⁷⁻²⁹) of electrons and holes in GaAsN. Therefore diffusion currents are neglected in the calculation.

In this case n_{\pm} and p are understood as the 1D local densities of electrons and holes, therefore $n_{\pm} \equiv n_{\pm}(t, x)$ and $p \equiv p(t, x)$. Similarly the number of paramagnetic impurities can be replaced by the local density of impurities $N_{\pm} \equiv N_{\pm}(t, x)$ and $N_2 \equiv N_2(t, x)$. $\mathbf{S} \equiv \mathbf{S}(t, x)$ and $\mathbf{S}_c \equiv \mathbf{S}_c(t, x)$ are the free electron and paramagnetic trap spin densities respectively.

The drift density current for electrons is $J_n = J_+ + J_-$ where $J_{\pm} = -\mu_e E n_{\pm}$ corresponds to spin up- and spin down-electrons. For holes the drift density current is $J_p = \mu_h E p$. Here μ_e and μ_h are the electron and hole mobilities respectively. They are set to $\mu_e = 200$ cm²/Vs and $\mu_h = 100$ cm²/Vs respectively as measured and calculated for similar samples²⁷⁻³⁰. We must also include the spin density current terms. According to Dyakonov *et al.*³¹, the spin polarization current density tensor, neglecting a small spin orbit contribution, can be written for electrons as

$$\mathbf{J}_S = - \left(\mu_e E + D \frac{\partial}{\partial x} \right) \mathbf{S}, \quad (27)$$

where D is the diffusion coefficient. Due to the small conduction electron mobility the diffusion term can be

neglected in Eq. (27) so that

$$\mathbf{J}_S \approx -\mu_e E \mathbf{S}. \quad (28)$$

Gathering all the terms we obtain the following system of equations

$$\begin{aligned} \dot{\mathbf{S}} - \mu_e \left(\frac{\partial E}{\partial x} + E \frac{\partial}{\partial x} \right) \mathbf{S} + \frac{\gamma_e}{2} (\mathbf{S} N_1 - \mathbf{S}_c n) \\ + \frac{\gamma_a}{2} \mathbf{S} (N_i - N_3) + \frac{1}{\tau_s} \mathbf{S} + \mathbf{S} \times \boldsymbol{\omega} = \Delta \mathbf{G}, \end{aligned} \quad (29)$$

$$\dot{\mathbf{S}}_c + \frac{\gamma_e}{2} (\mathbf{S}_c n - \mathbf{S} N_1) + \frac{1}{\tau_{sc}} \mathbf{S}_c + \mathbf{S} \times \boldsymbol{\Omega} = \mathbf{0}, \quad (30)$$

$$\begin{aligned} \dot{n} - \mu_e \left(\frac{\partial}{\partial x} \right) n E + \frac{\gamma_e}{2} (n N_1 - 4 \mathbf{S} \cdot \mathbf{S}_c) \\ + \gamma_a n (N_i - N_3) = G, \end{aligned} \quad (31)$$

$$\dot{p} + \mu_h \left(\frac{\partial}{\partial x} \right) E p + \gamma_h N_2 p + \gamma_b p N_3 = G, \quad (32)$$

$$\dot{N}_1 + \frac{\gamma_e}{2} (n N_1 - 4 \mathbf{S} \cdot \mathbf{S}_c) - \gamma_h N_2 p = 0, \quad (33)$$

$$\dot{N}_2 - \frac{\gamma_e}{2} (n N_1 - 4 \mathbf{S} \cdot \mathbf{S}_c) + \gamma_h N_2 p = 0, \quad (34)$$

$$\dot{N}_3 - \gamma_a (N_i - N_3) n = 0 - \gamma_b p N_3. \quad (35)$$

The density of photogenerated carriers is obtained by multiplying (7) or (8) by the Gaussian spatial distribution $\exp[-(x-x_0)^2/2s_x^2]/\sqrt{2\pi}s_x$ which specify the laser profile needed in transport simulations. The laser spot radius s_x is varied according to the experimental conditions. Even though the generation terms for transport carriers do not figure explicitly in the equations above, they are considered through the boundary conditions. The number of incoming electrons and holes on opposite sides of the sample are fixed for a given voltage and electrical current.

It is worthwhile mentioning that, while the expression for the local conservation of paramagnetic centers [Eq. (6)] remains unchanged, the charge conservation condition [Eq. (5)] is replaced now by the continuity relation

$$\frac{\partial}{\partial t} (n - p + N_2 + N_3) + \frac{\partial}{\partial x} (J_e - J_p) = 0. \quad (36)$$

As for the PL experiments it is convenient to define a parameter that allows us to pin the SDR phenomena. The transport SDR ratio, similarly to the photoluminescence SDR ratio, is thus the quotient of the time averaged density current in circular polarization (\bar{J}_+) to the time averaged density current in linear polarization (\bar{J}_X):

$$\text{SDR}_r = \frac{\bar{J}_+}{\bar{J}_X} \quad (37)$$

where explicitly $\bar{J}_{+,X} = \int_0^{t_{pp}} J_{+,X}(t) dt / t_{pp}$.

IV. RESULTS AND DISCUSSION

The rate Eqs. (20)-(26) were solved by fourth-order Runge-Kutta method. As initial conditions the amount

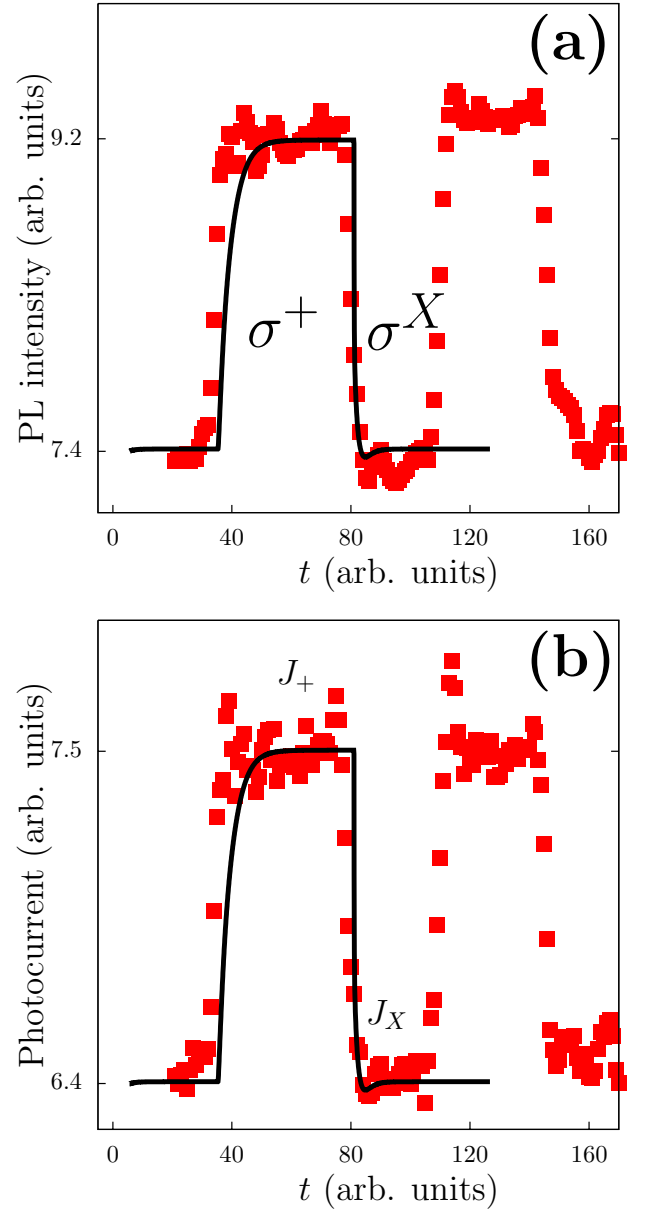


FIG. 2. (color online) (a) Photoluminescence intensity and (b) photocurrent signal as a function of time under circularly (σ^+) and linearly (σ^X) polarized light. The red squares indicate the experimental results for PL and PC and the thick black line represents the theoretical calculations.

of spin-up and spin-down electron on paramagnetic centers was set to $N/2$ while the remaining variables were set to zero.

In the transport case the carrier generation terms were introduced through the boundary conditions for a fixed voltage and current intensity; Dirichlet boundary conditions were imposed separately at the two ends of the sample for electrons and holes given that their distributions build up at opposite extremes. Accordingly, the space was discretized by forward and backwards differences for electrons and holes respectively. Initially the

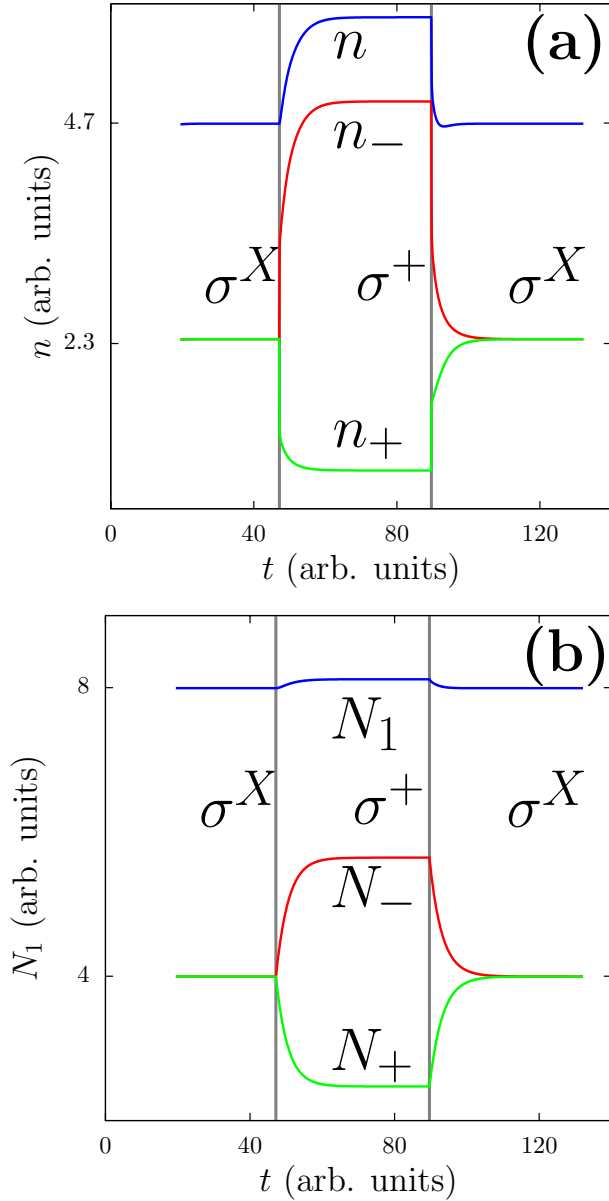


FIG. 3. (color online) (a) Spin-up n_+ (green), spin-down n_- (red) and total n (blue) density of free electrons. (b) Density of trapped electrons on paramagnetic centers: Spin-up N_+ (green), spin-down N_- (red) and $N_1 = N_+ + N_-$ (blue).

spin \mathbf{S}_c of trapped electrons was set to zero uniformly along the sample. As the mobility in GaAsN samples is very low it is possible to neglect the effects of transport in a first round of calculations using fourth-order Runge-Kutta method for each discretized position. The resulting system was solved by point Gauss-Seidel iteration method including the transport terms. In this calculations we used the same fitting parameters as the one introduced in Sec. III.

In Fig. 2 we present the simultaneous measurement of photoluminescence (a) and photocurrent (b) in sample B with lithographic contacts under CW excitation of

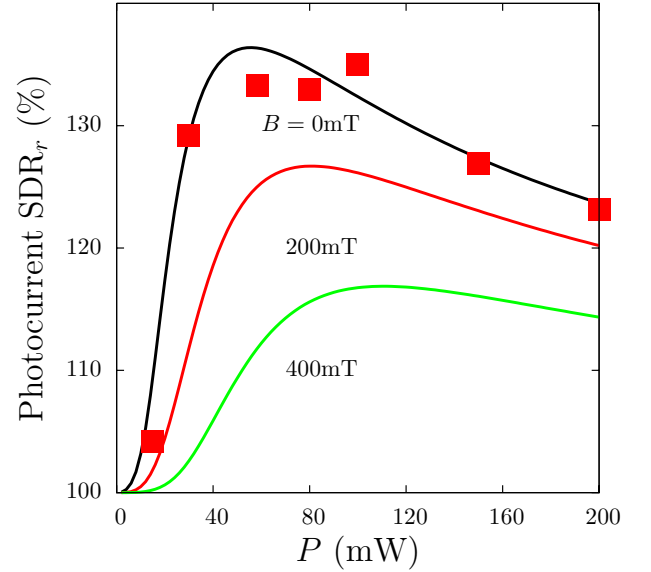


FIG. 4. (color on line) Photocurrent SDR_r vs laser irradiance P for different values of the magnetic field. The (red) squares are the experimental results, the dark solid lines indicate the theoretical curves for different transverse magnetic fields 0mT (black), 200mT (red) and 400mT (green).

$P = 5\text{mW}$. The (red) squares indicate the experimental measurement of PL and photocurrent while the solid lines correspond to the theoretical calculations obtained from the solution of the set of differential Eqs. (29)-(35). In this graph we observe an increase in the PL intensity under circularly polarized (σ^+) light compared to a linearly polarized excitation (σ^X). Likewise the photocurrent increases under a σ^+ excitation with respect to the σ^X case. A clear correlation is observed between the PL and PC behaviors. Under σ^X excitation the density of spin-up and spin-down polarized electrons are identical, namely $n_+ = n_-$ whereas with a σ^+ excitation n_- becomes considerably larger than n_+ [Fig. 3 (a)]. Through the dynamical polarization mechanisms the N_- to N_+ population ratio correspondingly follows the conduction band electron one [Fig. 3 (b)]. When $n_- \gg n_+$, the N_- density sharply increases, blocks further recombination of conduction band electrons of same spin orientation, and the N_+ population is depleted. Accordingly, for linearly polarized light we can see identical N_+ and N_- populations. The same model reproduces well the dependence of the PL and PC signal as functions of the excitation light polarization [solid line in Figs. 2 (a) and 2 (b)].

Fig. 4 [(red) solid squares] shows the photocurrent SDR_r as a function of power P under pulsed laser excitation for sample C whereas the solid (black) line represents the theoretical photocurrent SDR_r obtained from the set of differential Eqs. (29)-(35). Features identical to the PL experiments are measured and are precisely reproduced by the model.

In order to get further insight we studied the Hanle effect i.e. the depolarization of electrons in the presence

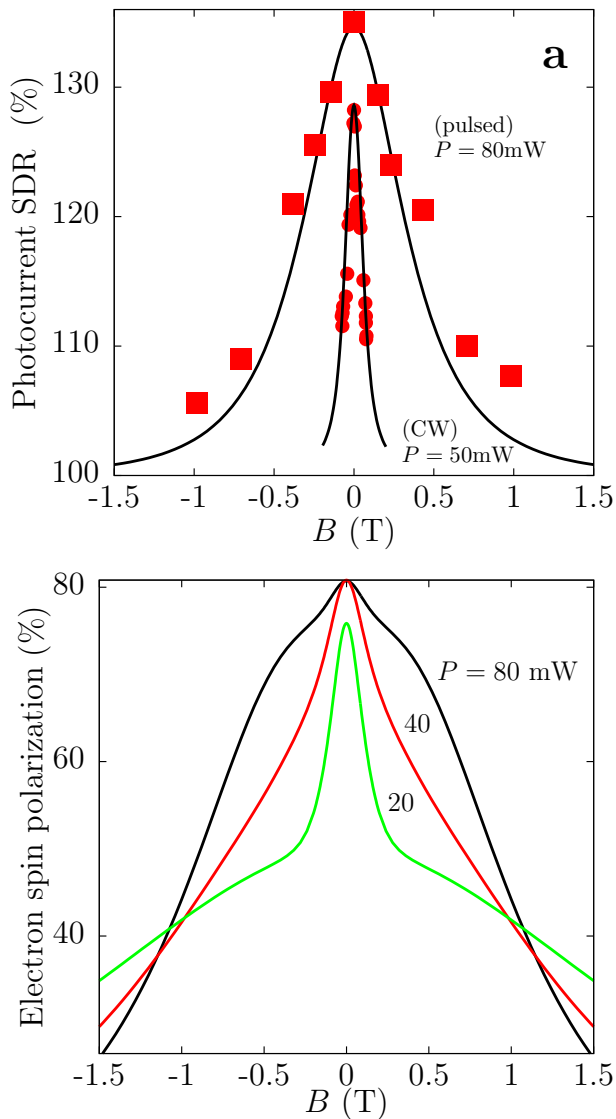


FIG. 5. (color on line) Hanle curve. (a) Photocurrent SDR ratio vs magnetic field B . The (red) squares display the experimental results for a power of 80mW in pulsed excitation and the (red) circles exhibit the experimental results at 100mW in CW excitation. The solid lines correspond to the theoretical calculations. (b) Theoretical values of the conduction band electron circular polarization P_c vs magnetic field B for $P = 80$ mW (black), 40 mW (red) and 20 mW (green) in pulsed operation.

of a magnetic field B in Voigt configuration³² and the consequent quenching of the SDR rate. For non vanishing values of the magnetic field (red for 200mT and green line for 400mT) a progressive decrease in the SDR_r is observed in Fig. 4 as expected. As the transverse magnetic field is increased the originally polarized spin of conduction band and trapped electrons begin to precess around the magnetic field with different angular velocities given the different g factors. The recombination through paramagnetic centers is thus triggered due to the dephasing

induced mismatch between spin of conduction band electrons and trapped electrons.

In Fig. 5 (a) we present the experimentally recorded variation of the SDR ratio as a function of an external magnetic field for sample C at $P = 80$ mW under pulsed excitation conditions. A very strong reduction of the photocurrent SDR ratio describing a quasi Lorentzian curve is observed. The model described in Sec. III B reproduces accurately the measured magnetic field dependence [(black) solid line in Fig. 5 (a)]. To clarify further the magnetic field dependence let us recall that in the simplest situation of an electron spin precessing around the external magnetic field, the Hanle effect yields a Lorentzian dependence for the electron spin polarization described by:

$$P_c = \frac{P_0}{1 + \left(\frac{B}{B_{1/2}}\right)^2} \quad (38)$$

where the half-width $B_{1/2}$ is given by^{21,32}

$$B_{1/2} = \frac{\hbar}{g\mu_B T_s}, \quad (39)$$

where T_s is the mean decay time:

$$\frac{1}{T_s} = \frac{1}{\tau_s} + \frac{1}{\tau} \quad (40)$$

and τ is the electron lifetime. We emphasize here that the data displayed in Fig. 5 (a) do not correspond to a classical Hanle curve which probes the spin depolarization in a photoluminescence experiment. Therefore, to interpret the experimental data, we have calculated in Fig. 5 (b) the free electron spin polarization degree as a function of the magnetic field B obtained from the model for various values of the power for circularly polarized (σ^+) excitation. This curve presents new features hidden in the SDR magnetic field dependence in PC. The curves show two superimposed Lorentzian with different half widths that strongly suggest two distinct processes with different mean spin life times. The magnetic field has here the double effect of depolarizing the conduction band and paramagnetic center resident electrons. Due to their significantly different spin lifetimes the B field dependence of the polarization shows the double Lorentzian curve as observed by Kalevich *et al.*³² in CW PL polarization experiments. For low excitation power the narrow Lorentzian is controlled by the localized electrons (long) spin life time while the larger Lorentzian corresponds to the free electron (short) spin life time. In the photoconductivity experimental results of Fig. 5 (a), the width of the curve is determined by the localized electron spin lifetime T_s which corresponds to the electron lifetime τ . The latter is controlled by the spin-dependent capture of free electrons (see Sec. III). To further support this interpretation we have measured the magnetic field dependence of the photocurrent at much lower photo-generated electron density (i.e. under CW excitation). As shown in

Fig. 5 (a) [(red) circles], the width of the curve is one order of magnitude smaller due to the longer localized electron lifetime³³. We emphasize that the same set of parameters were used in the calculations for Fig. 2, Fig. 4 and Fig. 5.

V. CONCLUSIONS

We have presented photoluminescence and photocurrent measurements in GaAsN samples that evidence the presence of many SDR related phenomena such as a spin dependent photoconductivity change and Hanle effect in the SDR ratio of the photoconductivity. We have found a strong correlation between photoluminescence and photoconductivity results. To get further insight on the interplay of the many different mechanisms involved we developed a model that correctly reproduces the main features of these phenomena. The model is based on a set of non-linear transport differential equations containing drift density currents for electrons and holes and terms that account for photogeneration, SDR in paramagnetic centers, and recombination through non paramagnetic centers. The presence of a constant magnetic field is introduced through spin-precession terms. First, we have shown that the interplay of SDR and non SDR channels is responsible for the most important features

of the SDR ratio vs laser irradiance curve. It presents a maximum that can be explained as a result of the competition between recombination through SDR and non SDR channels that activate at high laser pumping. As the recombination through non paramagnetic centers becomes more likely the maximum SDR ratio decreases. Second, we investigated the effect of a transverse magnetic field (Voigt configuration) on the Spin Dependent Photoconductivity. The SDR ratio vs magnetic field curve shows a Lorentzian-like shape which is reminiscent of the Hanle effect experienced by conduction band electrons and traps.

ACKNOWLEDGMENTS

This paper is dedicated to the memory of Naoufel Ben Abdallah. Alejandro Kunold acknowledges financial support from “Estancias sabáticas al extranjero” CONACyT and “Acuerdo 02/06” Rectoría UAM-A, to support his sabbatical stay from UAM-A in INSA Toulouse. Xavier Marie acknowledges the support of IUF and Cost Action n° MP0805. The support of QUATRAN(BLAN07-2 212988) funded by the French ANR and from the Marie Curie Project DEASE: MEST-CT-2005-021122 of the European Union is also acknowledged.

-
- ¹ S. Geschwind, R. J. Collins, and A. L. Schawlow, *Phys. Rev. Lett.* **3**, 545 (1959).
 - ² D. Lépine and J. J. Préjean, in *Proceedings of the 10th International Conference on the Physics of Semiconductors*, edited by S. P. Keller, J. C. Hensel, and J. Stern (Boston, 1970) p. 805.
 - ³ D. J. Lepine, *Phys. Rev. B* **6**, 436 (1972).
 - ⁴ T. Wosinski, T. Figielski, and A. Makosa, *Phys. Status Solidi (a)* **37**, K57 (1976).
 - ⁵ I. Solomon, D. Biegelsen, and J. C. Knights, *Solid State Commun.* **22**, 505 (1977).
 - ⁶ C. Weisbuch and G. Lampel, *Solid State Commun.* **14**, 141 (1974).
 - ⁷ D. Paget, *Phys. Rev. B* **30**, 931 (1984).
 - ⁸ M. Weyers, M. Sato, and H. Ando, *Jpn. J. Appl. Phys. Part 2 - Lett.* **31**, L853 (1992).
 - ⁹ A. Egorov, V. Kalevich, M. Afanasiev, A. Shiryaev, V. Ustinov, M. Ikezawa, and Y. Masumoto, *J. Appl. Phys.* **98** (2005).
 - ¹⁰ V. Kalevich, E. Ivchenko, M. Afanasiev, A. Shiryaev, A. Egorov, V. Ustinov, B. Pal, and Y. Masumoto, *Jetp Lett.* **82**, 455 (2005).
 - ¹¹ L. Lombez, P.-F. Braun, H. Carrère, B. Urbaszek, P. Renucci, T. Amand, X. Marie, J. C. Harmand, and V. K. Kalevich, *Appl. Phys. Lett.* **87**, 252115 (2005).
 - ¹² V. K. Kalevich, A. Y. Shiryaev, E. L. Ivchenko, A. Y. Egorov, L. Lombez, D. Lagarde, X. Marie, and T. Amand, *Jetp Lett.* **85**, 174 (2007).
 - ¹³ V. K. Kalevich, A. Shiryaev, E. Ivchenko, A. Y. Egorov, L. Lombez, D. Lagarde, X. Marie, and T. Amand, *Pis'ma v ZhETF* **85**, 208 (2007).
 - ¹⁴ F. Zhao, A. Balocchi, A. Kunold, J. Carrey, H. Carrere, T. Amand, N. Ben Abdallah, J. C. Harmand, and X. Marie, *Appl. Phys. Lett.* **95**, 241104 (2009).
 - ¹⁵ X. J. Wang, I. A. Buyanova, F. Zhao, D. Lagarde, A. Balocchi, X. Marie, C. W. Tu, J. C. Harmand, and W. M. Chen, *Nat. Mater.* **8**, 198 (2009).
 - ¹⁶ D. Kaplan, I. Solomon, and N. Mott, *J. Phys. Lett.* **39**, L51 (1978).
 - ¹⁷ R. Haberkorn and W. Dietz, *Solid State Commun.* **35**, 505 (1980).
 - ¹⁸ D. Lagarde, L. Lombez, X. Marie, A. Balocchi, T. Amand, V. K. Kalevich, A. Shiryaev, E. Ivchenko, and A. Egorov, *Phys. Status Solidi (a)* **204**, 208 (2007).
 - ¹⁹ E. L. Ivchenko, V. K. Kalevich, A. Y. Shiryaev, M. M. Afanasiev, and Y. Masumoto, arXiv:1008.4755v1.
 - ²⁰ F. Zhao, A. Balocchi, G. Truong, T. Amand, X. Marie, X. J. Wang, I. A. Buyanova, W. M. Chen, and J. C. Harmand, *J. Phys.-Condens. Matter* **21**, 174211 (2009).
 - ²¹ F. Meier and B. P. Zakharchenya, “Optical orientation,” (NorthHolland, Amsterdam, 1984).
 - ²² D. J. Hilton and C. L. Tang, *Phys. Rev. Lett.* **89**, 146601 (2002).
 - ²³ The bimolecular recombination process has thus been neglected in Eqs. (1)-(2).
 - ²⁴ X. J. Wang, Y. Puttisong, C. W. Tu, A. J. Ptak, V. K. Kalevich, A. Y. Egorov, L. Geelhaar, H. Riechert, W. M. Chen, and I. A. Buyanova, *Applied Physics Letters* **95**, 241904 (2009).

- ²⁵ G. Pettinari, F. Masia, A. Polimeni, M. Felici, A. Frova, M. Capizzi, A. Lindsay, E. P. O'Reilly, P. J. Klar, W. Stolz, G. Bais, M. Piccin, S. Rubini, F. Martelli, and A. Franciosi, *Phys. Rev. B* **74**, 245202 (2006).
- ²⁶ H. M. Zhao, L. Lombez, B. L. Liu, B. Q. Sun, Q. K. Xue, D. M. Chen, and X. Marie, *Applied Physics Letters* **95**, 041911 (2009).
- ²⁷ S. Fahy, A. Lindsay, H. Ouerdane, and E. P. O'Reilly, *Phys. Rev. B* **74**, 035203 (2006).
- ²⁸ W. Li, M. Pessa, J. Toivonen, and H. Lipsanen, *Phys. Rev. B* **64**, 113308 (2001).
- ²⁹ R. Mouillet, L.-A. de Vaulchier, E. Deleporte, Y. Guldner, L. Travers, and J.-C. Harmand, *Solid State Communications* **126**, 333 (2003).
- ³⁰ S. Fahy and E. P. O'Reilly, *Applied Physics Letters* **83**, 3731 (2003).
- ³¹ M. I. Dyakonov, *Phys. Rev. Lett.* **99**, 126601 (2007).
- ³² V. Kalevich, A. Shiryaev, E. Ivchenko, M. Afanasiev, A. Egorov, V. Ustinov, and Y. Masumoto, *Physica B* **404**, 4929 (2009).
- ³³ We measured a similar width of the classical Hanle curve determined by the polarization of the CW photoluminescence spectroscopy.